DII-6 THE FORMATION OF NECKING IN POLYCRYSTALLINE STEEL

P.S. Theocaris and E. Marketos(*)

A B S T R A C T

Tensile tests of thin-flat specimens of polycrystalline steel have been carried out at the vicinity of their ultimate tensile strength to determine the strain and stress distribution at the neighborhood of the neck.

The experimental analysis was restricted to the study of the first stage of a ductile fracture i.e. the study of the instability in balance between geometric and strain-hardening factors at the vicinity of the maximum tensile load with the subsequent initiation and formation of the neck.

Mechanical interference of crossed gratings photoprinted on the surface of thin-flat specimens, and similar reference gratings yielded the components of displacements along the principal directions of the specimens at the plastic domain of deformation.

Interference of a line grating superimposed on the specimen and obliquely illuminated and viewed, and its shadow on the matt reflective surface of the specimen allowed the evaluation of the thickness variation at the neighborhood of the neck. The combination of the two methods gave the state of deformation over a large gage area at various infinitesimal loading steps before and after the maximum tensile load and it proved to be very sensitive to strain variation.

The experimental study revealed important features of the phenomenon of instability of stresses and strains proceding the initiation of neck, as well as the subsequent appearance, evolution and stabilization of the position and size of the necked area.

I. I N T R O D U C T I O N.

The ideal fracture strength as determined from the atomic bond strength can be obtained only in especially prepared specimens, while ordinary samples usually fracture at much lower stresses. The reduction of fracture strength in brittle materials may be attributed to creation and development of cracks, which act as stress concentrators, while in the case of ductile materials plastic deformation occuring to some region of the solid enables the cross section of this area to diminish locally by its non uniform distribution.

(*) Professor and Assistant, National Technical University, Athens (147), Greece.

A ductile fracture of a tension specimen involves three successive events. The necking of the specimen, the formation of a small crack by accumulation of cavities at the necked region, and the final break of the specimen. The cavity, when becomes large enough, spreads fairly rapidly in a transverse direction at the interior of the specimen, occuping a large portion of the necked region. In the third stage the crack expands to the boundary following a direction inclined to about 45 deg. to the tension axis.

While several theoretical and experimental studies exist, which are related to the two final stages of fracture, the first stage, which is by far the most important and the longest, has been given less attention.

Koerber and Siebel[1] studied for the first time the mode of fracture of wide tension specimens. They attributed the oblique necking of their specimens to a simultaneous gliding on the two systems of slip planes.

Bijlaard[2] and separately Nadai[3] presented theories analyzing the mode of deformation contribution to the development of the oblique necking and determined an angle of necking of the order of 35 deg. Their analysis was based on the deformation theory and on a loading function which followed the energy of distortion criterion. They accepted that a state of plane stress prevailed at the vicinity of necking and assumed that necking of the specimen appeared when the ultimate load was applied to the specimen. The necking was considered as a stationary phenomenon with the component of strain parallel to the edges of the neck vanishing.

Thomas, in a series of papers[4], derived the same results and angles, as in the previous studies, without introducing assumptions extraneous to the basic equations of the theory. The theories advanced by Thomas concerned the processes of yielding in slip bands, but since the processes of yielding and breaking are closely linked in many forms of fracture, these results were extended to the case of necking of flat bars under tension.

The well known studies by Bridgman[5] were confined to determine the stress and strain distribution across the neck in cylindrical and flat specimens by measuring the radius of curvature of the neck contour and introducing approximate relationships for the components of strains which, based on experimental evidence, simplified considerably the analysis.

Throughout the previously described work the instability phenomenon of local yielding and necking was treated as a quasi-static equilibrium phenomenon, related to the ultimate tensile strength of the sample because it was assumed that necking appears when this load is reached. Thus, the general dynamic conditions of equilibrium were reduced to simple relations with the speed of propagation of necking assumed equal to zero. Moreover Hencky's stress-strain relations, which were used by most of the studies did not allow for redistributions of the components of strains with eventual negative increments due to elastic recovery in regions far from the moving strain fronts producing the necking.

Hill[6] studied the permissible discontinuities of stress velocity and surface slope in a plastic-rigid plate satisfying any type of plastic

potential and yield function. It has been shown that one such discontinuity of velocity may be taken as an idealization of localized neck of the thin sheet.

In a recent review paper by Low[7] the microstructural aspects of ductile fracture were discussed. It was shown in a series of recent investigations by Plateau et al[8], Puttick(9), Cottrell(10) and Rogers(11) that the ductile fracture resulted from rupture by void formation in the heavily deformed region at the tip of an advancing ductile crack. But, while the experimental evidence from the studies by Cottrell, Puttick, Plateau et al. was convincing that foreign particles and inclusions are a common nucleating site for cavities, Rogers observed that cavities may be nucleated in regions severely deformed, but without any indication of existence of inclusions. Moreover Beevers and Honeycomb(12) found no evidence of cavity formation in a series of experiments with high purity aluminum. They concluded that severe slip bands produced cracks, which resulted in failure.

All these studies were related primarily to the second and final stages of crack formation and rupture of the specimens.

This paper deals with the mechanism of plastic instability of tension specimens leading to the initiation and consequent formation of the necking. Thin-flat specimens made of a steel alloy were tested in pure tension up to their necking. Crossed gratings photoprinted on their surfaces yielded, by mechanical interference with similar reference gratings, the components of displacements along the principal axes. Successive infinitesimal steps before necking gave all the necessary data for the complete evaluation of the strain components at each loading step. The experimental analysis allowed the complete study of the phenomenon of necking.

II. BASIC RELATIONS

The analysis of the experimental results was based on the incremental theory of plastic deformation and the Prandtl-Reuss stress-strain relations were adopted. This was implied by the nature of the problem, where negative strain increments were anticipated in the vicinity of the neck, due to partial elastic recovery in these regions.

Introduction of the Hencky stress-strain relations, although it could make the analysis less formidable, should not be applied to the problem since there was not a unique correspondence between stresses and total strains.

Prandtl-Reuss relations, expressing the plastic increments of strain $d\varepsilon^p_{ij}$ in terms of the deviatoric components of stress s_{ij}, are given by the relation

$$d\varepsilon^p_{ij} = s_{ij}\, d\lambda \qquad (1)$$

where $d\lambda$ is a scalar factor of proportionality. Prandtl-Reuss relations (1) combined with Mises' yield function give the following relation

$$d\varepsilon^{p}_{ij} = \frac{3\, s_{ij}\, d\bar{\sigma}}{3\,\bar{\sigma} H'} \qquad (2)$$

where H' is the slope of the effective stress $\bar{\sigma}$ versus plastic strain curve.

Since we are concerned with the strain and stress distribution at the vicinity of the neck it is reasonable to neglect the elastic components of strains and to accept plastic incompressibility. Indeed, for the material used in the tests (U.S. Steel T 1) it was shown(13) that the value of the lateral contraction ratio reaches 0.5 in earlier stages of plastic deformation.

Then, the stress-strain relations used in calculations may be written as follows:

$$d\varepsilon^{p}_{x} = d\lambda\left[\sigma_x - \frac{1}{2}(\sigma_y + \sigma_z)\right], \quad d\gamma^{p}_{yz} = 3d\lambda\tau_{yz}$$

$$d\varepsilon^{p}_{y} = d\lambda\left[\sigma_y - \frac{1}{2}(\sigma_x + \sigma_z)\right], \quad d\gamma^{p}_{zx} = 3d\lambda\tau_{zx} \qquad (3)$$

$$d\varepsilon^{p}_{z} = d\lambda\left[\sigma_z - \frac{1}{2}(\sigma_x + \sigma_y)\right], \quad d\gamma^{p}_{xy} = 3d\lambda\tau_{xy}$$

For the flat parts of the surface of the specimens, as well as for the bottom lines of the necks, the σ_z-component of stress normal to the surface vanishes.

Relations (3), solved in terms of the stress-components for $\sigma_z = 0$, yield the following equations:

$$\sigma_y = \frac{2}{3d\lambda}(2d\varepsilon^{p}_{y} + d\varepsilon^{p}_{x}) \qquad \tau_{zx} = \frac{1}{3d\lambda}\, d\gamma^{p}_{zx}$$

$$\sigma_x = \frac{2}{3d\lambda}(2d\varepsilon^{p}_{x} + d\varepsilon^{p}_{y}) \qquad \tau_{yz} = \frac{1}{3d\lambda}\, d\gamma^{p}_{yz} \qquad (4)$$

$$\sigma_z = 0 \qquad \tau_{xy} = \frac{1}{3d\lambda}\, d\gamma^{p}_{xy}$$

The coefficient of proportionality $d\lambda$ is given by the relation (2) that is

$$d\lambda = \frac{1}{H'} \cdot \frac{d\bar{\sigma}}{\bar{\sigma}} \qquad (5)$$

The values of this coefficient may be determined for each point of the specimen and each loading step from the effective stress $(\bar{\sigma})$-effective strain $(\bar{\varepsilon})$ curve of the material.

For the complete solution of the strain-and stress - distribution at the vicinity of the neck the load was raised to a step where the limit of uniform strain distribution is slightly exceeded at the whole gage area of each specimen. This could be readily checked by observing

the shape of the moiré fringes produced.

Then, a process of a succession of infinitesimal increments of load was adopted, in order to follow the variation of the strain-and stress-distribution during the initiation and formation of the neck.

Five loading steps will be discussed in the following analysis. The two first steps corresponded to loadings antecedent the maximum load. The third step was referred to the ultimate tensile strength, while the two last steps were related to the evolution and stabilization of the position of the neck.

III. EXPERIMENTAL PROCEDURE

The specimens tested in this investigation consisted of thin sheets of a low-carbon high-yield-strength alloy steel under commercial designation U.S.S. T 1'. The chemical composition of the material was as follows: C 0.15, Mn 0.79, P 0.015, S 0.016, Si 0.24, Cr 0.52, Ni 0.88, Cu 0.24, Mo 0.46, V 0.05, B 0.003%. The metallic sheets were water quenched from 1650/1750° F and tempered at 1150/1275° F. This type of steel alloy was chosen because it presents a reduced work hardening, which helps considerably the formation of neck. Moreover, previous experience showed that the fine grained metallic sheets of this alloy did not present an appreciable anisotropy at several directions (less than 3%).

The specimens were cut as longitudinal samples from larger and thicker plates and were machined to a uniform thickness of 4 mm. The width of the plate at mid-length was 90 mm. and a small taper of an angle of 2 deg. to the longitudinal axis was given in both directions in order to produce a minimum section at the mid-length of the specimen (Fig. 4).

The two tapered parts of each longitudinal boundary were joined with an arc of circle of a radius of 270 mm. In this way the small fillet produced, while it assured a minimum section where the neck was forced to appear, it did not produce any stress concentration. The length of the specimens was taken equal to 700 mm.

The last layer of each flat surface of a thickness of 0,25 mm was removed by slow grinding with a well lubricated porous wheel in order to avoid any increase of temperature. The longitudinal axis of the specimens was coïnciding with the rolling direction of the plates. One surface of each specimen and the part corresponding to the gage area had a ground finish taken down to "0000" emery paper and it was polished afterwards with diamond paste. Thus, the surface was made free from pits, scratches or other imperfections.

Great care was taken in aligning the specimen in the grips of the testing machine. The alignment was checked by loading each specimen at the vicinity of the yield point and observing the emerging moiré fringes from the one extremity of the gage area to be parallel lines. This proved to be a very sensitive way of checking the alignment.

The testing machine used was a 100 ton Amsler hydraulic testing machine having a capacity considerably larger than that of the specimen.

Therefore, the effects of inertia of the weighing mechanism, as well as the elasticity of the different parts of the testing machine on the shape of the stress-strain curves were very small. Crosshead speads were kept constant all over each test and very low, interrupted by constant load intervals for taking photographs at each loading step. The deformation speed was controlled by the speed of emergence of the moiré fringes.

The testing machine was fitted with axial loading shackles especially designed to assure alignment of the applied load by allowing free rotation in three mutually perpendicular directions in both shackles. Self-alignment was obtained through arrangements of thrust bearings and ball joints in each shackle.

The moiré method was used for the measurement of the components of displacements along the principal axes of the specimen. A model grating was reproduced on the ground surface of the specimen by using the photoprinting method. The model grating was an orthogonally crossed grating of a density of 20 lines per mm. in both directions. To this grating a reference line grating was superimposed twice successively in the two principal directions. The density of the reference grating was the same as the model grating in its underformed state. Since we were interested to large plastic strains at the vicinity of the neck the two identical gratings before loading gave dense patterns after loading the specimen.

The mechanical interference of the deformed model grating and the reference grating gave moiré fringes which measured the displacement components along both principal directions of the specimen. Figs. 1 (a & b) show the displacement fields in both directions as they were depicted by the moiré fringes before the initiation of the neck, Figs 2 (a & b) present the moiré patterns in the fifth step of loading where the neck is already formated.

In order to measure the thickness variation at the vicinity of the neck and to check the results of the analysis the shadow moiré method was applied(14). For this purpose a reference line grating of a density of 16 lines per mm. (different from the density of the model grating to avoid any mechanical interference between the two gratings) was placed to ride on the high points of the necked specimen. The combination of the grating and the matt reflecting surface of the specimen was illuminated by collimated white light under a certain angle of incidence.

The reference grating and its shadow interfered and produced a moiré pattern, which yielded the thickness deformation arising from the Poisson effect. Fig. 3 shows the moiré pattern produced by this method at the vicinity of the neck.

IV. RESULTS

Five characteristic loading steps were chosen from the series of incremental steps done during each test. The two first steps corresponded to applied loads inferior than the maximum load and to steps of

deformation prior than the deformation corresponding to the ultimate strength. The third step corresponded to the maximum load and the subsequent two steps were related to the appearance and the evolution of the neck.

The determination of the strain-and stress-components was executed in fourteen transverse and longitudinal sections on the surface of the specimens for each loading step. The various sections are presented in Fig. 2. In cases where the strain-and stress-distribution were of a similar shape in the two halves of the specimen the values of these components at the upper half appeared in the discussion of results.

a) S t r a i n s : The longitudinal ε_y-and the transverse ε_x-strains are depicted in Figs 5 to 8. In these figures the strain-distribution is presented for the five successive loading-steps and along four sections parallel to the minimum section x_o-x_o of the specimens.

It is clear from these diagrams that the ε_x-strain distribution is basically similar to the ε_y-strain distribution. The curves of the y- and x-strains are convex downward at the middle of the x_o-x_o section for loads preceding the maximum load P_{max}. This distribution degenerates progressively to the inverse distribution with withdrawal from the minimum section. The same conclusion may be deduced from Fig.9, where the curves of equal ε_y-strain distribution appear for the three first steps of loading.

The ε_y-strains are continuously increasing with increasing applied load. For steps beyond P_{max} a further increase of the strain-components appears in the region of the necks, while a decrease of strains occurs in regions remote from necks. The strain decrease starts from the interior of the specimen, while an increase of strains is still manifested at the bound aries. Further decrease of the external load influence the ε_y-strain distribution at the boundaries, which then follow the decrease of ε_y-strains at the interior. The maximum decrease is limited to the elastic component of deformation. It is clear from Fig. 8 that the maximum of strains happens along the longitudinal axis passing through the point of the crossing of the necks.

For loads preceding or equal to P_{max} increase of the ε_y- and ε_x-strains at the vicinity of the minimum section and close to the free boundaries results in a strain-distribution which appears to be locally concave to the neutral axis. Local protrusions in the strain-distribution appear at the vicinity of the boundaries, which move as moderate strain-waves from the free boundaries to the interior. Simultaneously, they increase in value following the increase of the external load. The non-uniform strain distribution across any transverse section becomes more severe for the maximum load P_{max} and increases further for the subsequent steps of loading. The tops of the moving strain-protrusions end to the severe local raisings of Figs. 5 to 7 for the final steps which correspond to the already visible necks.

It may be concluded from the above analysis that this occurence, which predicts the initiation of the necks and the subsequent fracture,

appears long before the applied load reaches its maximum value.

Another important observation is that the neck first appears in places different from its final position and it moves progressively toward its final position with the evolution of the applied load.

Fig. 9 shows the ε_y-strain distribution on the surface in three characteristic loading steps. The evolution of the phenomenon is followed during the interval when a longitudinal strain of the order of 70 x 10^{-3} mm/mm appears first and then disappears from the gage area studied. It is worthwhile noting that the maxima of ε_y-strains move continuously, while they increase with the applied load from the free boundaries to the interior. This movement is followed by the neighboring strains in a V-shape with the apex of the angle coinciding with the position of the maximum deformation and oriented toward the longitudinal axis. The angle of the V-shape was measured to be of the order of 29 deg.

In this manner the apices of the ε_y-strains, moving from the free boundaries to the interior from both sides of the longitudinal axis, merge at the vicinity of this axis forming a double necking.

Fig. 10 presents the distribution of the ε_y-strains during the last loading step. Three necks appear in this figure, which according to their size are characterized as primary, secondary and tertiary neck. The strain distribution along the necks is strongly non-uniform. The apparently non-symmetric shape of necks and the presence of a tertiary neck may be attributed either to a small eccentricity of the external load or to a non-symmetric and non-uniform strain distribution due to geometrical or strain-hardening factors, or, finally, to a combination of all these factors.

The initiation of the visible necks with severe plastic deformations of the order of 130 x 10^{-3} mm/mm does not occur at their final position. The bottoms of the necks, where the maximum strains appear, move like moderate waves, in the same manner as the previously described movements of the maxima of the instability strain concentrations, towards the interior. This phenomenon may be deduced from Fig. 10 where the isoentatics (lines of equal strain) appear denser at the edges of the neck lying at the interior of the specimen, which is the direction of movement of the neck, and sparser in the regions where the moving strain-wave has already passed.

Thus, the movement of strain protrusions continues in the form of compression after the occurence of the necks. The angle formed between the axes of necks with the transverse axis of symmetry of the specimen was equal to $\pm$ 29 deg.

Fig. 11 presents the evolution of ε_y-strains along the lines $\alpha\beta$ and $\alpha'\beta'$ which define the bottom lines of the necks during the last step of loading. It is clear from these diagrams that there is no significant difference between the ε_y-strains along the two bottom lines during the first two steps. On the contrary, there is a distinct difference between the strain distribution along these lines for the step N° III. This difference becomes more severe in the last loading step. As it is expected at the crossing point of the two necks the ε_y-strain takes equal values.

Until the step N° IV the coalescence of the two from both sides moving protrusions has not been accomplished. In the final step, when this coalescence has been taken place, an abrupt increase of the curve of strain distribution occurs. The dotted lines in Fig. 11 show the shape of the curves of the ε_y-strain distributions just before the coalescence of the two protrusions.

Then, it may be concluded that the strain protrusion becomes remarkably intense at the area of coalescence of the two protrusions with the result that the specimen produces a visible neck and reaches there closer the point of rupture of continuity of the material then in any other part.

The difference in the strain distribution along the two necks accounts for the distinction of the neck $\alpha\beta$ as the primary neck and the neck $\alpha'\beta'$ as the secondary neck.

The rupture of the specimen takes finally place along the primary neck under an angle of 29 deg. to the transverse axis of the specimen. This type of fracture was expected since the width of the specimen is larger than 20 times its thickness. It is known that when the ratio of the width to the thickness of a tension thin-flat specimen is larger that five, the neck is produced not to a transverse direction but to an oblique angle(3).

Fig. 12 shows the shear strain distribution on the surface of the specimen. Shear strains take small values and they slightly increase during the loading steps preceding the formation of neck. The shear strain distribution is uniformly and smoothly changing. It becomes wavy and larger during the final step of the initiation of the neck.

b) S t r e s s e s : The components of σ_y- and σ_x-stresses were determined by applying relations (4) and assuming that the material follows Mises' loading function. These components of stresses were plotted for the first four steps in Figs. 13 to 16.

The evolution of the σ_y-stress distribution for the steps preceding $P_{max.}$ is rather smooth. The non-uniformity in the stress distribution at $P_{max.}$ becomes apparent and for the last step of the initiation of neck the stress distribution turns into a severely non-uniform distribution with fluctuations in the values of stresses in comparison with the previous steps.

The maxima of stresses for steps I and II appear at the interior in contrast to the corresponding distribution of strains, which present their maxima at the boundaries. The maximum stresses move with the increase of loading to their future positions at the necks.

It may, then be deduced that for loads smaller than the load corresponding to step I the distribution of stresses may present a maximum value at the middle of the specimen, which is split into two parts moving

towards the necks as the external load is increasing. Thus, it may be concluded that the instability phenomena, which generate the initiation and development of necking and which are related to non-uniform strain and stress distributions in parts of the specimen, appear long before the maximum load is reached.

With the decrease of the external load, which follows the maximum load, the maximum values of stresses continue to increase, while the same stresses start to decrease far from the necking regions. This decrease appears first in places remote from the necks and it speads to regions closer and closer to the necks with the progressive decrease of the external load.

The transverse σ_x-tension stresses are equal to zero at the free boundaries and they present the shape of a saddle along any transverse section with two maxima in both sides of the longitudinal axis. With the appearance of the neck these maxima are displaced to the bottom lines of the necks and the relative minimum between them tends toward the secondary neck.

c) P l a s t i c w o r k: The plastic work per unit of volume W_t was determined by using the relation

$$W_t = \int_s dw$$

where dw is the elementary plastic work defined by the equation:

$$dw = \sigma_{ij}\, d\varepsilon_{ij} \qquad (6)$$

The total plastic work W_t is found from dw by integration along each deformed transverse section. The distribution of the plastic work at the various sections is shown in Figs 17 and 18.

Fig. 17 presents the evolution of the difference of the total plastic work $(\Delta(\Sigma W_t))$ between the loading steps for the transverse sections x_ox_o, x_2x_2 and x_3x_3. The work is expressed as percentage of the every time value of the difference at the minimum section x_ox_o. It is clear from this figure that, during the evolution of the phenomenon of instability and necking, the increase of the dissipated plastic work is continuous in any section and this increase is more severe along the minimum section than along any other transverse section.

The distribution of the total plastic work (ΣW_t) follows a similar law as the previously described but with smoother change from the maximum to the minimum values. This quantity for the five loading steps is depicted in Fig. 18. Again the total plastic work is normalized to the value of the plastic work at the minimum section corresponding to the maximum load $P_{max.}$ The reduction of the plastic work outside the minimum section is considerable. Thus, for the last loading step and at a distance from the section x_ox_o equal to 0.40 of the minimum width the plastic work takes a value equal to the half of its maximum value.

If we assume that the width of the specimen is constant and the distribution of the plastic work in the direction of loading is uniform for

the loading step corresponding to $P_{max.}$, then, the plastic work distribution for the subsequent steps is presented by the dotted lines of Fig.18. Then, again for the last step N° V we have at the section $x_3x_3(0.40xd_{min})$ that the plastic work is equal to 0.70 of the plastic work corresponding to $P_{max.}$

V. CONCLUSIONS

A study of the mechanism of plastic instability of thin-flat tension specimens made of low-carbon steel alloys was undertaken in this paper. The phenomenon of plastic instability and the subsequent phenomenon of initiation, evolution and stabilization of the position and size of the necks produced was studied by measuring the components of strains all over the gage area by applying the moiré method.

It was shown that the instability phenomenon starts and continues over a large range of strain and stress preceding and following the maximum external load. The initiation of the instability in a specimen is related to a specific configuration of the deformed body, which depends on the mode of distribution of plastic strains at a load approaching the maximum external load, which the specimen is assigned to sustain.

The initial non-uniformity in the strain distribution, which appears long before the maximum load is reached, is continuously changing with the evolution of loading. Local protrusions in the strain-distribution appear at the vicinity of the free boundaries, which move like moderate strain waves toward the interior, while, simultaneously, they increase in value.

The movement of the maxima of the longitudinal strains is followed by the neighboring strains in a V-shape wave, which moves from both sides of the free boundaries to the interior. When these strain waves merge at the vicinity of the longitudinal axis they form a double neck.

When the neck is well developed one system of slip lines, corresponding to the so-called primary neck, begins to pre-dominate over the other systems.

The localized severe deformation, associated with the neck formation, governs the phenomenon of further evolution of the necking. Indeed, the state of plastic deformation is the principal factor influencing the mode of initiation, formation and the final shape of the neck, while the applied load and the stress distribution derived from are only necessary to characterize this state of plastic deformation. The rate of work hardening of the material associated with the localized severe plastic deformation at the necked area are the main factors controlling the mode of development of the necks.

The stress and strain distribution along the predominating system of slip, corresponding to the primary neck, continues to increase over the secondary neck, producing a higher resolved shear stress on this plane. This leads to a deeper neck observed at the final step of loading, which may lead for further loading to the formation of a ductile

crack, which, once formed, it may readily propagate because of the favorable stress conditions at the neck.

Again, the position of the initiation of the necks does not coincide with their final position. The bottoms of the necks move slowly to the interior as the strain concentration is increasing presenting a steeper interior edge and a smoother exterior edge which prove their slight movement towards to longitudinal axis of the specimen.

The stress-distribution during the initiation of neck is severely non-uniform with fluctuations in the values of stresses presenting their maxima at the bottom lines of the necks.

Similarly, the distribution of the dissipated plastic work presents similar shapes with severe increase of the dissipated plastic work at the vicinity of the neck and simultaneous relaxation at regions distant from the necks.

ACKNOWLEDGMENT

The experimental work contained in this paper was sponsored by the U.S. Department of the Army through its European Office, under contract DA-91-591-EUC-3347. The support of this agency is gratefully acknowledged.

REFERENCES

1. Koerber F. & Siebel E., Naturwissenschaften, 16, 408 (1928).

2. Bijlaard, P.P., Rept. Intern. Ass. Bridge & Struct. Engrg., 6, 27 (1940).

3. Nadai, A., Theory of Flow and Fracture of Solids, Second Edition, McGraw-Hill Book C°, N.Y., 319 (1950).

4. Thomas, T.Y., Plastic Flow and Fracture in Solids, Academic Press N.Y. 102, (1961).

5. Bridgman, P.W., Studies in Large Plastic Flow and Fracture, First Edition, McGraw-Hill Book C° Inc., N.Y., 9 (1952).

6. Hill, R., J.Mech. Phys. Solids, 1, 19 (1952).

7. Low, J.L., Jr., Fracture of Solids, D.C.Drucker and J.J.Gilman, Eds., Interscience Publ., 197 (1962).

8. Plateau J., Henry G. and Crussard C., Rev. de Metallurgie 54, 200 (1957).

9. Puttick K.E., Phil. Mag., 4, 964 (1959).

10. Cottrell A.E., Fracture, B.L. Averbach, D.K. Felbeck, G.T. Hahn

and D.A. Thomas, Eds., Wiley, N.Y., 20 (1959).

11. Rogers H.C. Trans. A.I.M.E., 218, 498 (1960).

12. Beevers C.J. and Honeycombe R.W.K., Phil Mag., 7, 763 (1962).

13. Theocaris P.S. and Koroneos E., Phil. Mag., 8, 95, 1871 (1963).

14. Theocaris P.S., J.Sci. Inst., 41, 133 (1964).

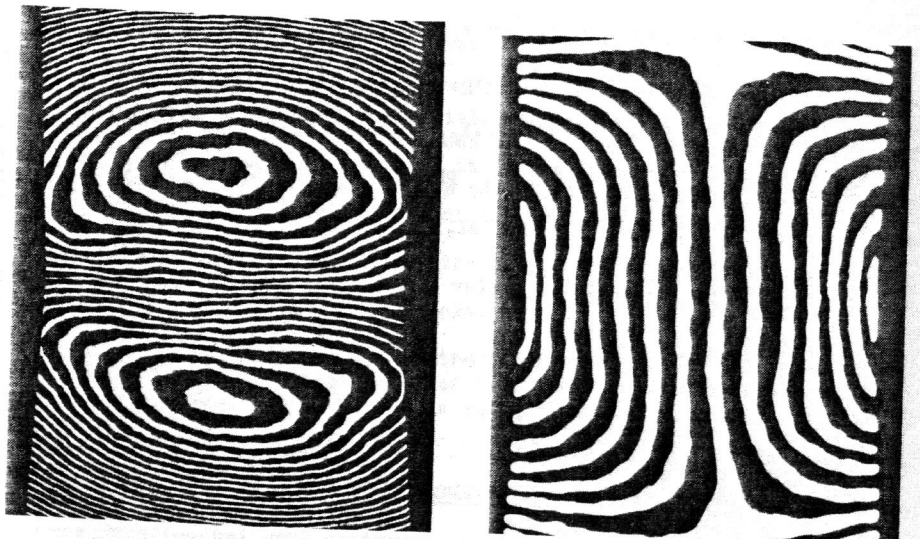

(a) (b)

FIG. 1 (a & b) Moire patterns of the displacement fields along the axes of symmetry of the tension specimen at a loading step antecedent the maximum load.

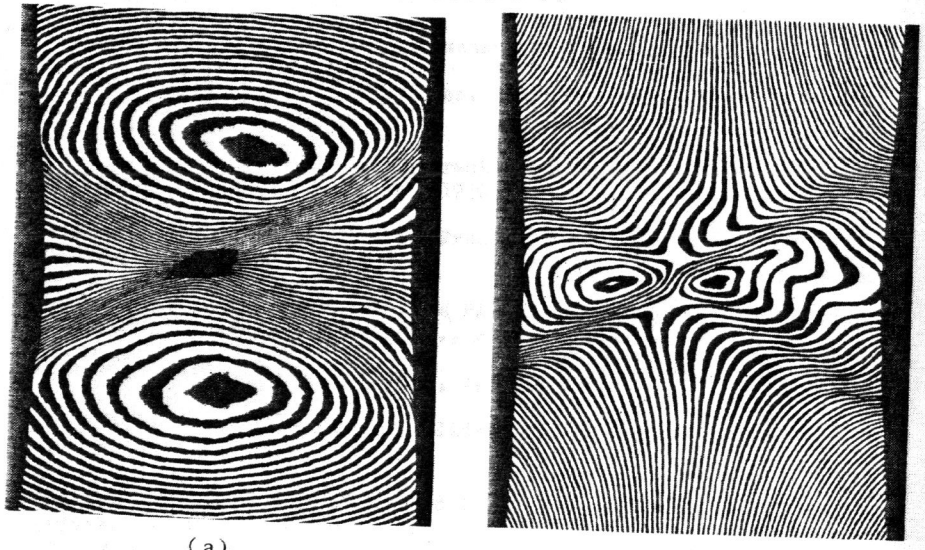

(a) (b)

FIG. 2 (a & b) Moiré patterns of the displacement fields along the axes of symmetry of a tension specimen at a loading step coinciding with the formation of a triple neck.

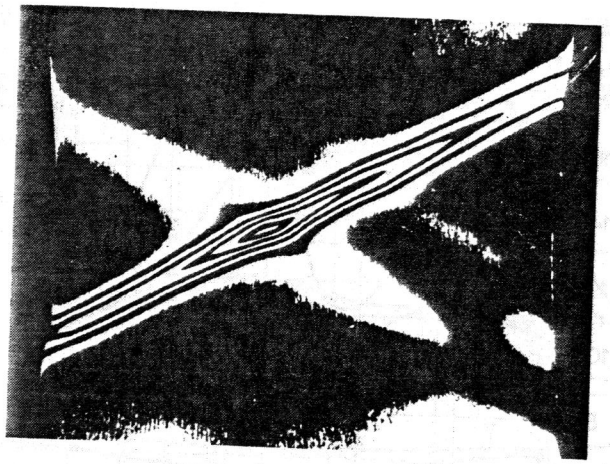

FIG. 3. Moiré pattern showing thickness contours of the necked tension specimen.

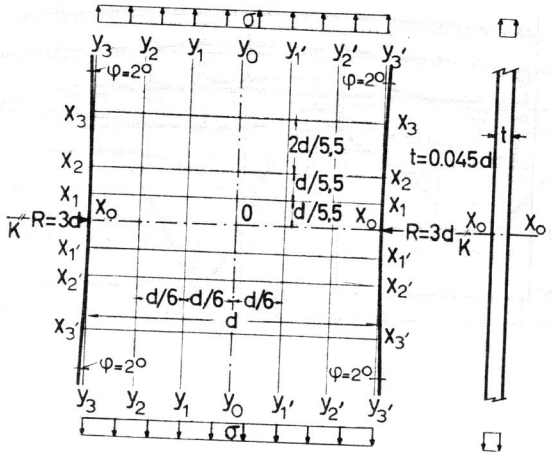

FIG. 4. Gage area of the tapered tension specimen.

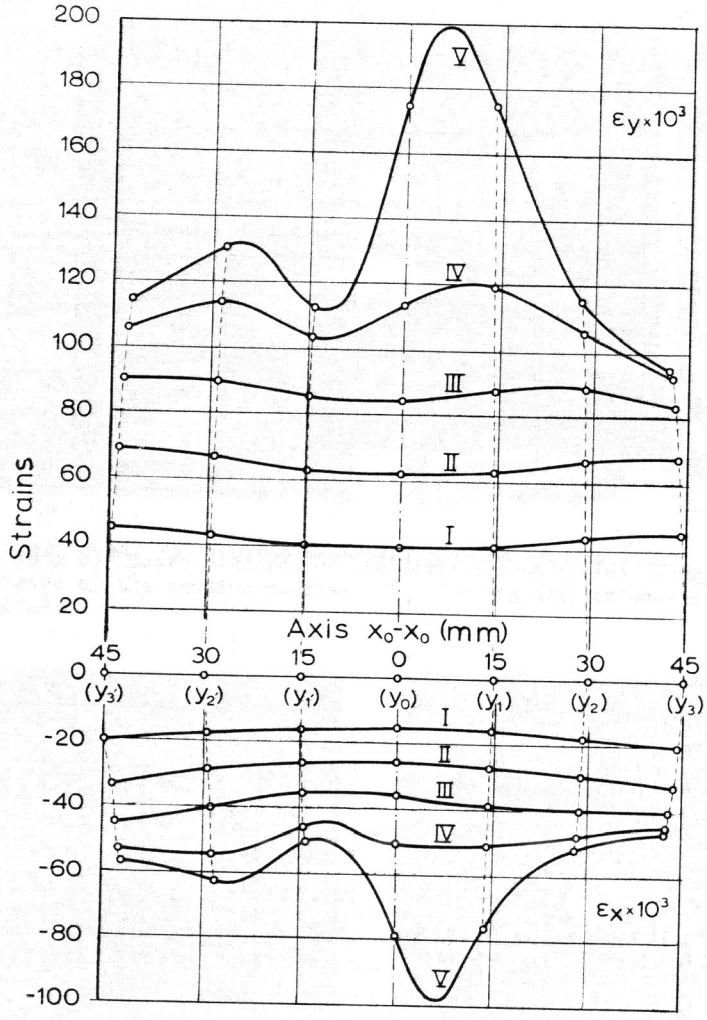

FIG. 5. Longitudinal (ε_y) and transverse (ε_x) strain distribution at the transverse section x_0x_0 of the tension specimen for the five loading steps.

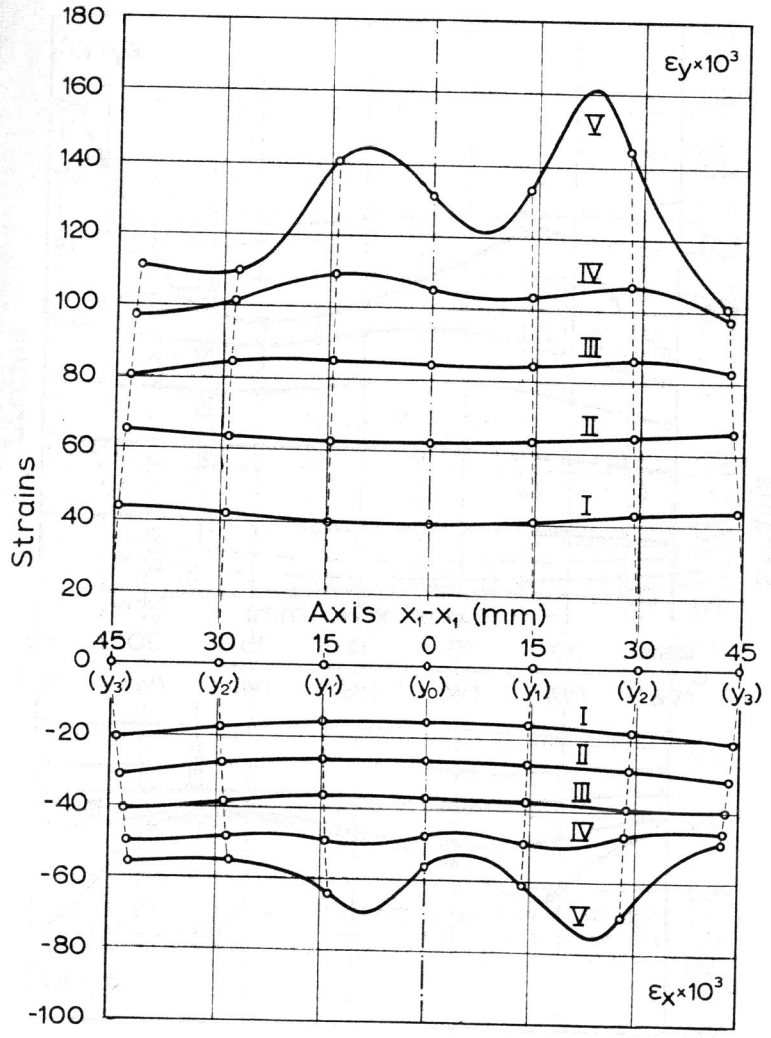

FIG. 6. Longitudinal (ε_y) and transverse (ε_x) strain distribution at the transverse section x_1x_1 of the tension specimen for the five loading steps.

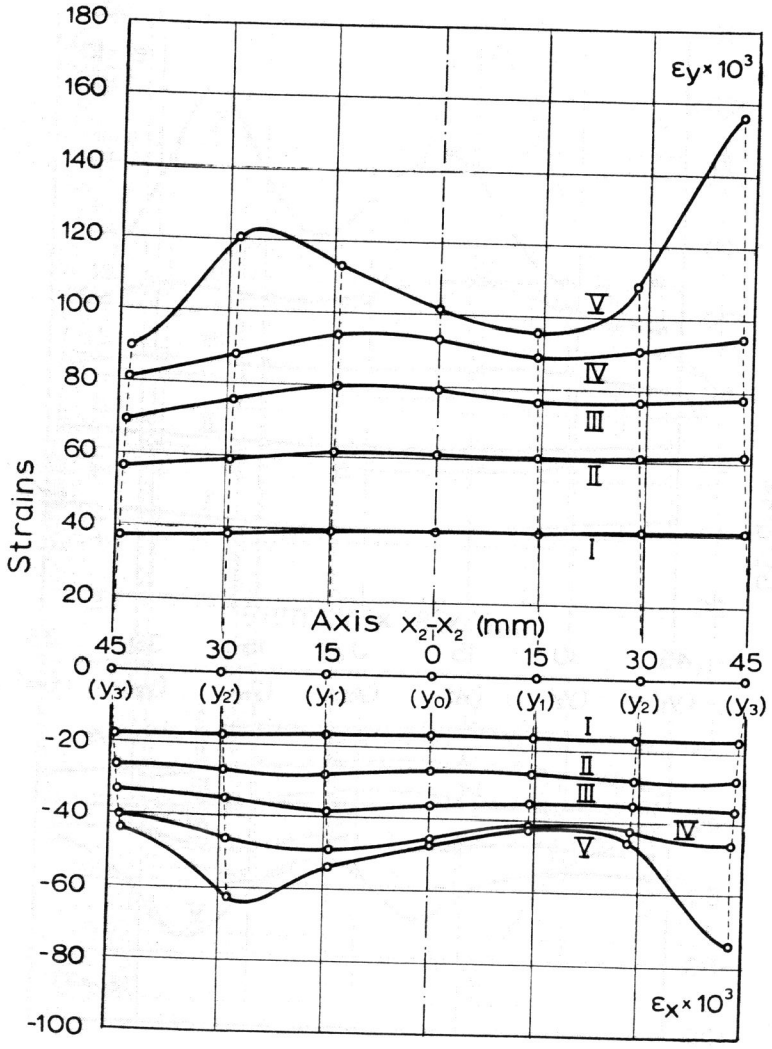

FIG. 7. Longitudinal (ε_y) and transverse (ε_x) strain distribution at the transverse section x_2x_2 of the tension specimen for the five loading steps.

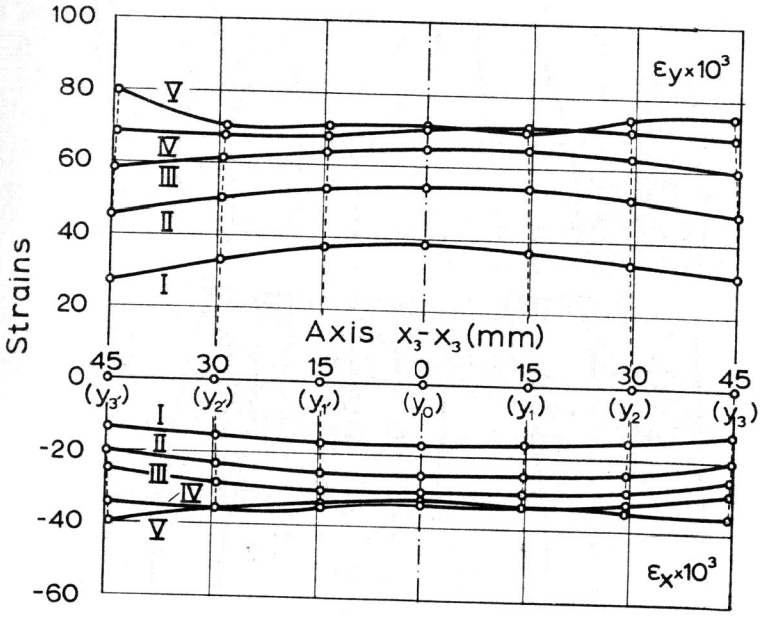

FIG. 8. Longitudinal (ε_y) and transvers (ε_x) strain distribution at the transverse section x_3x_3 of the tension specimen for the five loading steps.

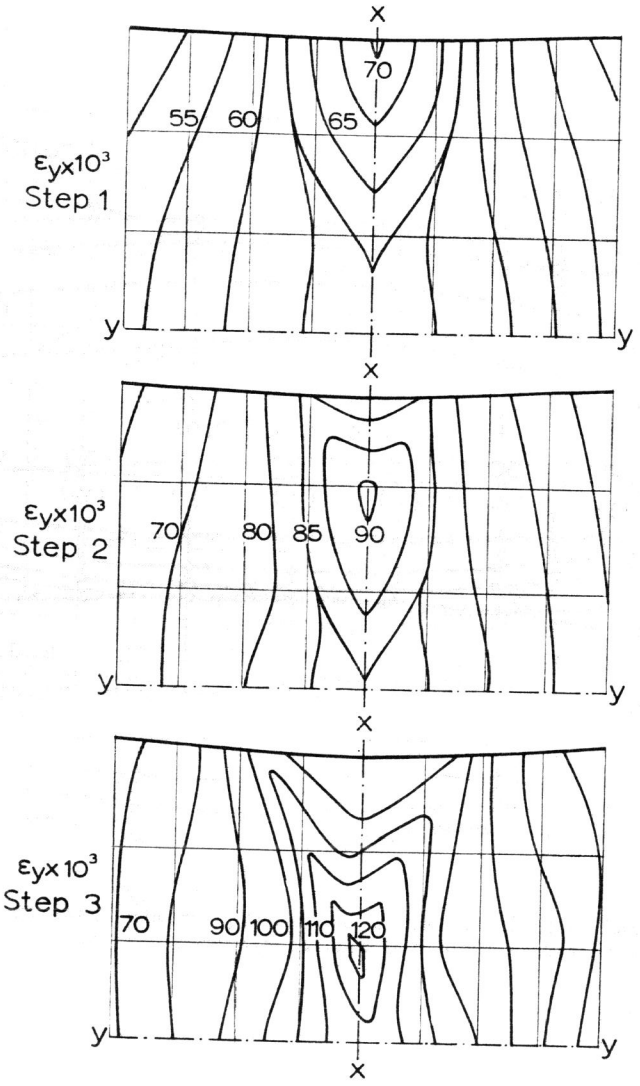

FIG. 9. Isoentatics of the ε_y-strain distribution for the first three loading steps.

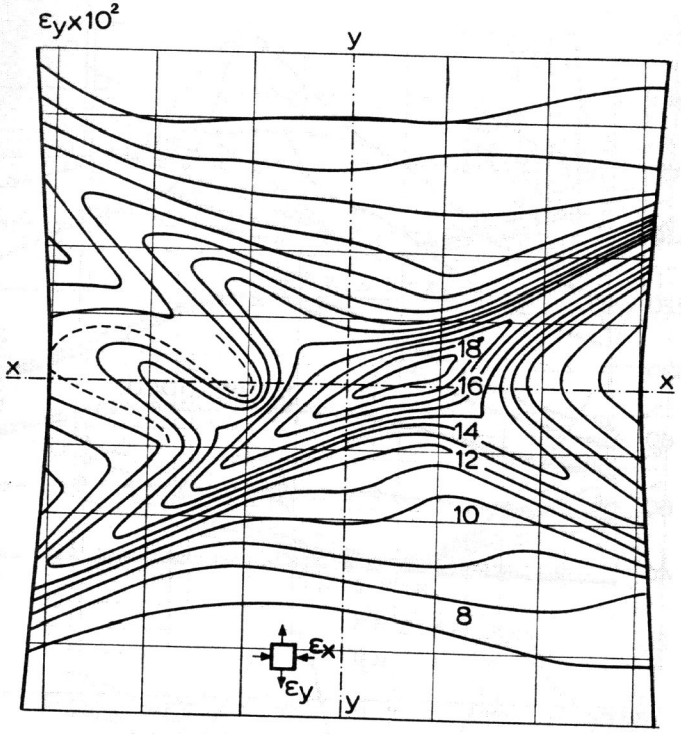

FIG. 10. Distribution of the ε_y-strains during the last loading step where necking is already formated.

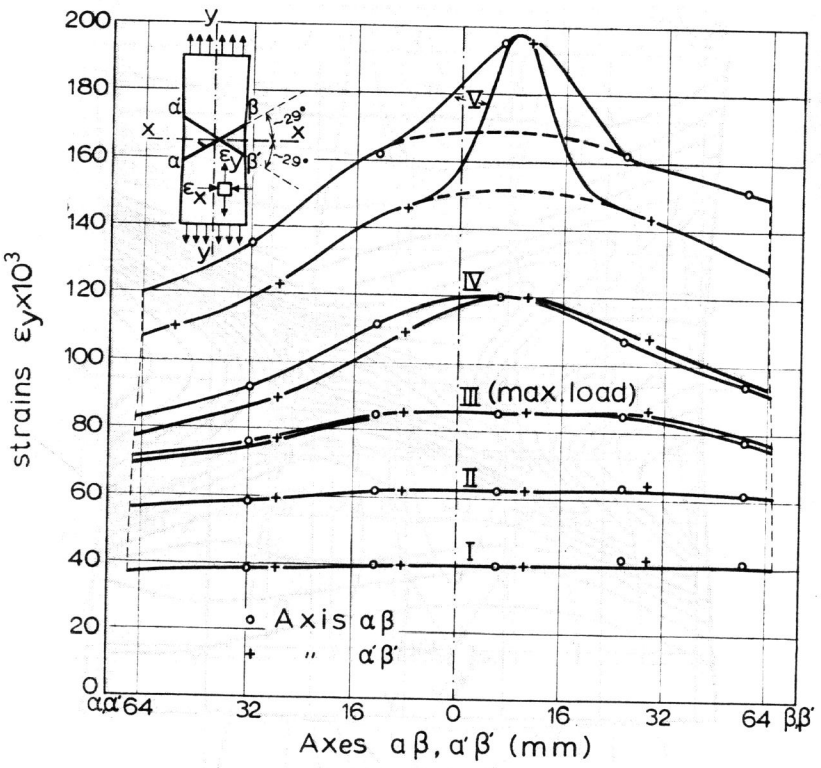

FIG. 11. Evolution of ε_y-strain distribution along the bottom lines of the primary ($\alpha\beta$) and secondary ($\alpha'\beta'$) necks.

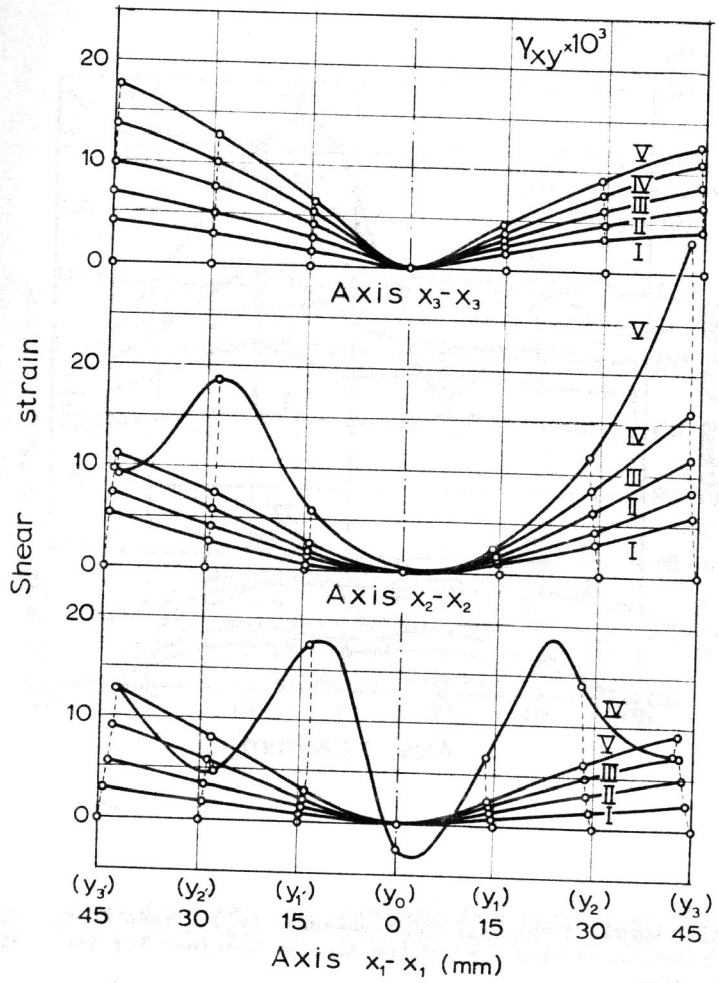

FIG. 12. Evolution of γ_{xy}-strain distribution at the transverse section x_0x_0 x_2x_2 x_3x_3 of the tension specimen for the first four loading steps.

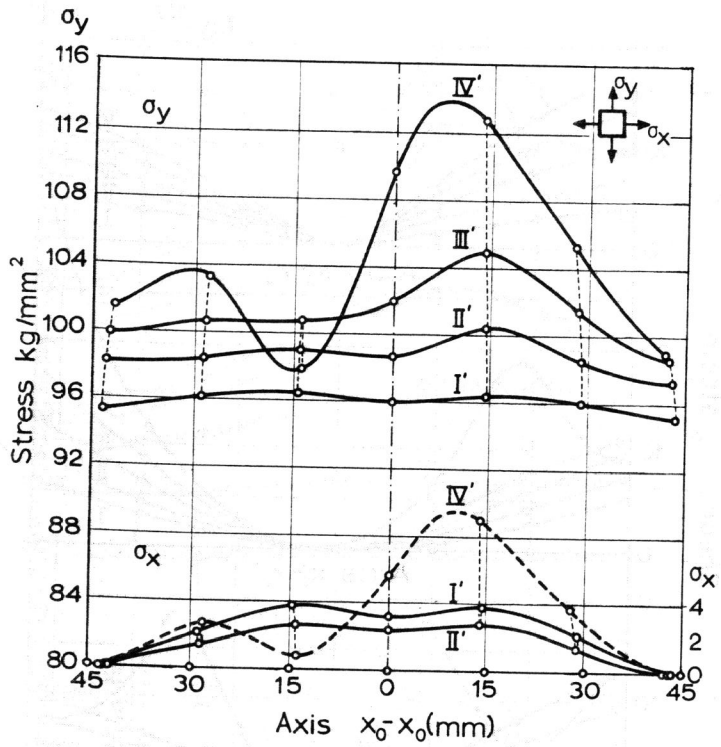

FIG. 13. Longitudinal (σ_y) and transverse (σ_x) stress distribution at the transverse section x_0x_0 of the tension specimen for the first four loading steps.

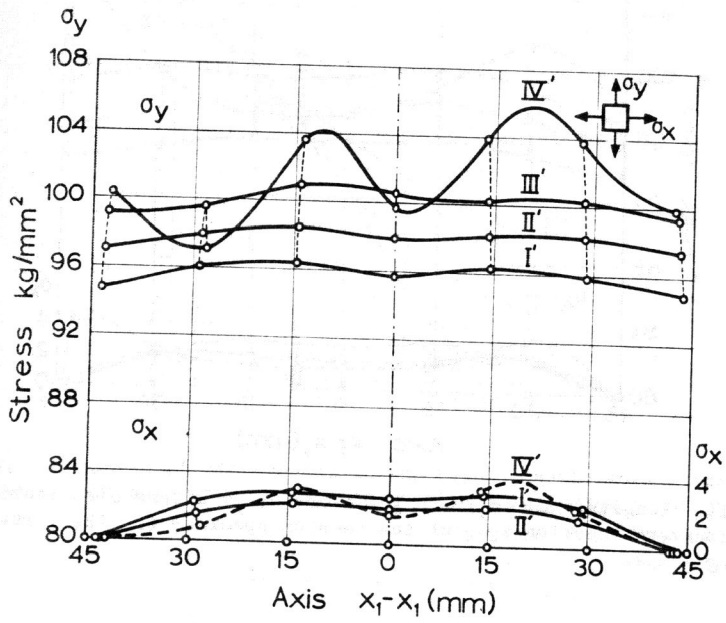

FIG. 14. Longitudinal (σ_y) and transverse (σ_x) stress distribution at the transverse section x_1x_1 of the tension specimen for the first four loading steps.

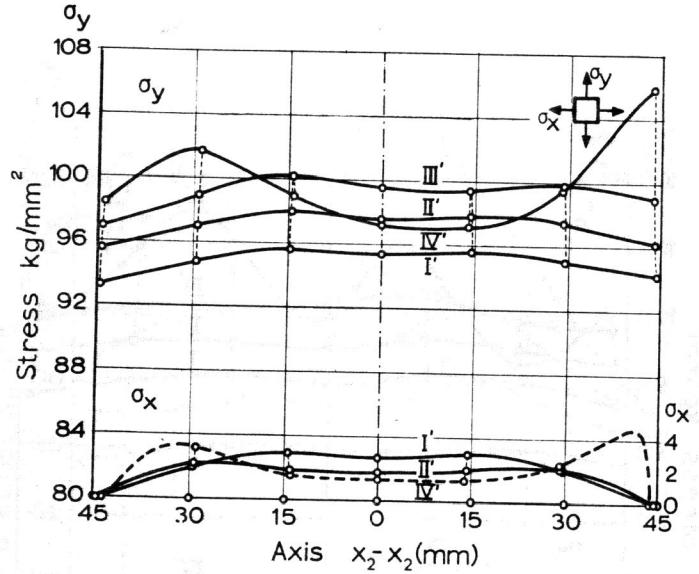

FIG. 15. Longitudinal (σ_y) and transverse (σ_x) stress distribution at the transverse section x_2x_2 of the tension specimen for the first four loading steps.

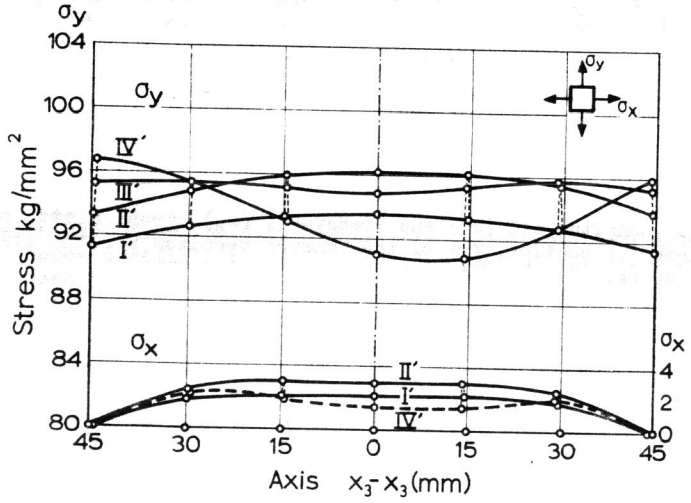

FIG. 16. Longitudinal (σ_y) and transvers (σ_x) stress distribution at the transverse section x_3x_3 of the tension specimen for the first four loading steps.

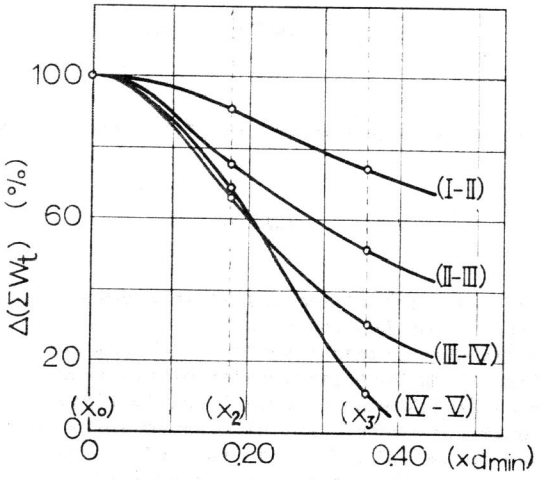

FIG. 17. Evolution of differences in the total plastic work between the five loading steps for the transverse sections x_0x_0, x_2x_2 and x_3x_3.

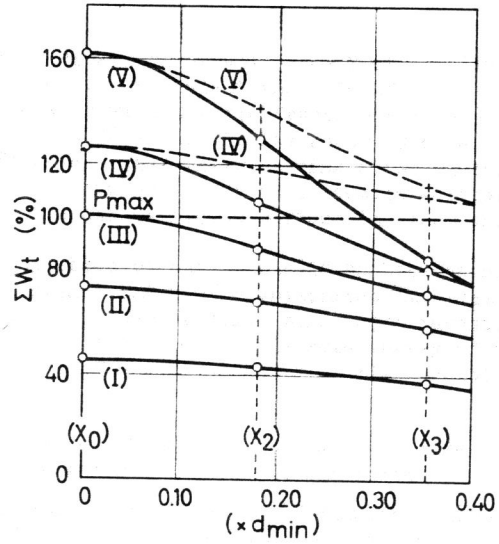

FIG. 18. Distribution of the dissipated plastic work for the transverse sections x_0x_0, x_2x_2 and x_3x_3 during the five loading steps.